Histol Histopathol (2007) 22: 527-534

http://www.hh.um.es

Histology and Histopathology

Cellular and Molecular Biology

Expression of annexin AI in conventional renal cell carcinoma (CRCC) correlates with tumour stage, Fuhrman grade, amount of eosinophilic cells and clinical outcome

U. Zimmermann[1], C. Woenckhaus[2], S. Teller[3], S. Venz[3,4], M. Langheinrich[3], C. Protzel[1], S. Maile[5], H. Junker[3] and J. Giebel[5]

[1]Department of Urology, Ernst Moritz Arndt University Greifswald, Greifswald, Germany, [2]Institute for Pathology, Ernst Moritz Arndt University Greifswald, Greifswald, Germany, [3]Department of Medical Biochemistry and Molecular Biology, [4]Laboratory for Functional Genomics, Ernst Moritz Arndt University Greifswald, Greifswald, Germany and [5]Institute for Anatomy, Ernst Moritz Arndt University Greifswald, Greifswald, Germany

Summary. There is increasing evidence that Annexin AI (ANX AI) expression is dysregulated in several carcinomas and tumour cell lines. In order to gain insight into the putative role of ANX AI in tumorigenesis, clinical outcome and metastatic potential of conventional renal cell carcinomas (CRCCs) we investigated the expression of ANX AI in CRCCs and metastases. Furthermore, it was elucidated whether ANX AI overexpression affects migratory potential in Caki-1 cells.

ANX AI immunohistochemistry was performed on 33 samples of CRCCs and 10 metastases. ANX AI expression was assessed in 12 samples by 2-dimensional gelelectrophoresis (2-DE), subsequent mass spectrometry and RT-PCR. Immunohistochemical data were statistically correlated with pathological parameters, amount of eosinophilic cells and clinical outcome. Furthermore, a haptotactic migration assay was done on Caki-1 cells transfected with ANX AI.

Immunostaining for ANX AI was found in 18 tumours and all metastases investigated. Intensity of immunohistochemical staining correlated to Fuhrman grade, amount of eosinophilic cells and clinical outcome. 2-DE and RT-PCR confirmed the presence of ANX AI in neoplastic tissue. Overexpression of ANX AI did not significantly influence cell migration.

From these findings ANX AI expression seems to be related to Fuhrman grade, clinical outcome and metastatic potential of CRCCs. Thus ANX AI could serve as a prognostic marker for tumour progression.

Offprint requests to: U. Zimmermann MD, Department of Urology, Ernst-Moritz-Arndt University, Fleischmannstrasse 42-44, 17475 Greifswald, Germany. e-mail: ziuro@uni-greifswald.de

Key words: Annexin AI, Kidney, Cancer, Immunohistochemistry, Cell Migration

Introduction

Annexin AI (ANX AI) is a member of a multigene family of Ca^{2+} and phospholipid binding proteins. Annexins are characterized by highly α-helical and tightly packed protein core domain, building a conserved Ca^{2+}-regulated membrane binding module. These proteins are present in the cytosol or associated with plasma or intracellular membranes and cytoskeletal proteins. Annexins are involved in regulation of ion channel activities, endocytotic and exocytotic processes, signal transduction, cellular differentiation and proliferation (Gerke and Moss, 2002; Gerke et al., 2005). ANX AI has been shown to participate in manifold physiological processes e.g. regulation of inflammation by inhibiting phospholipase A2, cell proliferation and cell migration (Masaki et al., 1994; Hayes and Moss, 2004; Perretti et al., 2002). Furthermore, overexpression of ANX AI is induced by heat, oxidative stress or by sulfhydryl-reactive agents (Rhee et al., 2000). In diffuse gastric carcinoma ANX AI is overexpressed compared to normal gastric epithelial tissue and intestinal-type gastric cancer (Wu et al., 2006). In hepatocellular carcinoma ANX AI upregulation is involved in transformation processes and related to histological grading (Masaki et al., 1996). On the other hand, downregulation of ANX AI was shown in prostate carcinoma (Kang et al., 2002; Lehnigk et al., 2005). Moreover, in head, neck and oesophageal squamous cell carcinoma, ANX AI down regulation is related to poor differentiation of tumours and thus to unfavourable

prognosis (Xia et al., 2002; Garcia Pedrero et al., 2004).

Although anti-ANX AI antibodies were previously detected in blood sera from renal carcinoma patients, and ANX AI was shown to be overexpressed in 5 out of 6 renal tumour samples, as shown by 2-DE (Unwin et al., 2003a,b), there is still little information on the role of ANX AI in renal carcinomas. This is all the more interesting since renal cancer accounts for 2-3% of all diagnosed malignancies and up to 95 000 deaths per year worldwide (Vogelzang and Stadler, 1998). Histologically 70% of all renal cell carcinomas are classified as conventional renal cell carcinomas (CRCC), characterized by the occurrence of clear, chromophobe and eosinophilic cells, although to different extents (Reuter and Gaudin, 1999). As shown recently, the amount of eosinophilic cells increased in higher grade lesions and correlated significantly with clinical outcome. Moreover, a relation between number of eosinophilic cells and expression of ANX AII was supposed. As the expression correlated to Fuhrman grade and clinical outcome, ANX AII was hypothesized to serve as a prognostic marker for the outcome of CRCC (Zimmermann et al., 2004).

In the present study, we investigated the expression of ANX AI in primary CRCC and metastases by immunohistochemistry. We also carried out 2-DE and mass spectrometry and reverse transcription polymerase chain reaction (RT-PCR) in homogenates of neoplastic and non-neoplastic tissues. Moreover, after ANX AI was overexpressed in Caki-1 cells the effect on migratory potential was investigated in a haptotactic migration assay.

Material and methods

Tissue samples

The study was based on CRCC samples obtained from 33 patients undergoing radical nephrectomy. Among these patients, 15 had metastases in lung (3), suprarenal gland (2), liver (3), bone (3), brain (1), lymph nodes (2) and skin (1). We investigated 10 metastases by immunohistochemistry – lung (2), suprarenal gland (2), liver (2), bone (1), brain (1), lymph node (1) and skin (1). Representative neoplastic and non-neoplastic tissue samples allowing proper classification and grading were fixed in 4% buffered formaldehyde. For 2-DE and qualitative RT-PCR different samples from 12 patients were snap frozen in liquid nitrogen and stored at -80°C until use. Tissue samples and patient data were obtained and used after advice from the ethics committee of the University of Greifswald and in accordance with the declaration of Helsinki. Follow-up data were collected from patient's records.

Histological methods and classification of tumours

Typing and classification were performed on specimens stained with hematoxylin and eosin (H&E). All specimens underwent additional independent histopathological review (C.W.). Tumours were classified as recommended by the latest TNM classification and graded according to Fuhrman et al. (Fuhrman et al., 1982; Sobin and Wittekind, 2002). The proportion of eosinophilic cells was assessed in all primary tumours by two independent observers (C.W., J.G.) and scored as E0 (<10%), E1 (11–30%), or E2 (>30%).

Immunohistochemistry

Immunohistochemistry was carried out on paraffin sections (4 µm). In detail, after deparaffinization according to standard protocol, endogenous peroxidase activity was blocked (Peroxydazed-1, Biocarta, Hamburg, Germany) (5 min, 22°C) and sections were subjected to heat for antigen retrieval (10 mM citrate buffer, pH 6.0). After cooling in citrate buffer and subsequent washings in PBS, immunohistochemistry was done using the 4 plus™ Universal Immunoperoxidase Detection System (Biocarta). Incubation with a monoclonal anti-ANX AI-antibody (Zymed, Berlin, Germany) was performed for 45 min at 22°C. After washing (PBS, 2x5 min), incubation with the secondary antibody was for 10 min at 22°C. Slides were washed in PBS (2x5 min) and subjected to streptavidin-HRP solution (Biocarta, 45 min). Visualization was achieved after washing (PBS, 2x5 min) with 0.1% diaminobenzidine in PBS/0.01% H_2O_2 followed by hematoxylin counterstaining, dehydration and mounting in Neomount (Merck, Darmstadt, Germany). Controls were done by i) incubating slides with PBS alone, ii) by using PBS instead of primary antibody, and iii) by replacing the ANX AI antibody with a monoclonal antibody (ß1-integrin, Biomol, Hamburg, Germany) which is not reactive on paraffin sections. Photographs were taken on an Olympus BX50 microscope equipped with an Olympus DP 10 digital camera. Staining intensity was judged by two independent observers (C.W., J.G.) and scored A0 (no reaction), A1 (strong staining at the cell membranes and no or weak reaction in the cytoplasm), and A2 (strong staining at the cell membrane and cytoplasm).

Two-dimensional gel electrophoresis (2-DE)

The preparation of protein samples was performed with the TRIzol®Reagent (Invitrogen, Karlsruhe, Germany) according to the manufacturer's protocol. Finally, the vacuum dried protein pellet was dissolved in sample buffer (8 M urea, 4% CHAPS, 65 mM DTT, 40 mM Tris). Amounts of protein were quantified by the Bradford method (Bradford, 1976). Samples were applied to IPG strips (pH 3-10 non linear, 24cm, Amersham-Bioscience, Uppsala, Sweden) by in-gel rehydration. A total of 500-750 µg protein was filled to a volume of 450 µl with rehydrating buffer [8 M urea, 2 M thiourea, 2% CHAPS, 10 mM dithiothreitol and 0.5% IPG-buffer, pH 3-10NL, Amersham Biosciences)]. After rehydration overnight, isoelectric focusing (IEF) was

carried out at 20°C on the PROTEAN IEF Cell (Bio-Rad) for a total of 55000 Vhr. Subsequently the IPG strips were stored at -20°C or immediately soaked twice in a solution containing 6 M urea, 375 mM Tris-HCl (pH 8,8), 20% glycerol, 2% SDS and 1% DTT for the first, or 2.5% iodoacteamide for the second step of equilibration. As tracking dye, a few grains of bromophenol blue were added. Strips were placed on vertical SDS-PAGE gels and overlaid with 1.0% agarose. SDS-PAGE was carried out using the PROTEAN plus Dodeca Cell (Bio-Rad), with gels of 1.5 mm thickness and an acrylamide concentration of 12.5%. After electrophoresis, gels were fixed in a solution of 15% acetic acid/40% methanol and stained with Colloidal Coomassie Blue (Roth, Karlsruhe, Germany) following the manufacturer's protocol.

Preparation of peptide mixtures for Matrix assisted Laser Desorption ionization mass spectrometry (MALDI-MS)

Proteins were excised from Colloidal Coomassie Blue stained 2-D gels using a spot cutter (Proteome Works™, Biorad, Hercules, CA, USA). Digestion with trypsin and subsequent spotting of peptide solutions onto the MALDI-targets were performed automatically in the Ettan Spot Handling Workstation (Amersham-Biosciences, Uppsala, Sweden) using a modified standard protocol as described elsewhere (Eymann et al., 2004). The MALDI-TOF measurement of spotted peptide solutions was carried out on a Proteome-Analyzer 4700 (Applied Biosystems, Foster City, CA, USA). After calibration, a combined database search of MS and MS/MS measurements was done using the GPS Explorer software (Applied Biosystems). Peak lists were compared with the IPI database (International Protein Index) compiled by the EBI (European Bioinformatics Institute) to provide a top level guide to the main databases that describe the human and mouse proteomes: SWISS-PROT, TrEMBL, NCBI RefSeq and Ensembl; restricted to human taxonomy using the Mascot search engine (Matrix Science Ltd, London, UK). Peptide mixtures that yielded a mowse score of at least 59 were regarded as positive identifications.

Cell migration assay

Transfection with full length ANX AI lead to a high degree of spontaneous apoptosis associated with caspase-3 activation (Solito et al., 2001). Therefore, a bioactive ANX AI N-terminal fragment (15S) was used for migration experiments (Perretti et al., 2002). Enhanced Green Fluorescent Protein (EGFP-ANX AI) transfection was generated by cloning a part of the coding region of the human ANX AI, to generate a peptide spanning from aa 1 to aa 136, into the vector pEGFP-N2 (Clontech, Palo Alto, USA). ANX AI (15S) DNA (Accession number NM_000700) was amplified by PCR using PWO DNA polymerase (PEQLAB, Erlangen, Germany) and the pRc/CMV-ANX A1 (15S) vector, kindly provided by Egle Solito (Imperial College School of Medicine, London, UK). The forward primer (5'-CCGCTAGCTA**CTCGAG**CATGGCAATGGTAT CAGAATTC-3') carried a XhoI restriction site (bold) and the reversed primer (5'-CCGATCACTT**CCG CGG**ATGATCTTCATCAGTTCCAAG-3') a SacII site (bold). Insertion of the XhoI/SacII digested PCR fragment into the XhoI/SacII restriction sites of the vector resulted in a C-terminal fusion of the ANX AI (15S) DNA to the EGFP cDNA. The correct sequence of the cloned PCR fragment was confirmed by sequencing (Seqlab, Göttingen, Germany). Haptotactic cell migration assays were performed in Transwell chambers (Costar Inc.: #3422, Cambridge, USA) according to Zhang et al. (2002). Membranes were coated at the bottom surface with vitronectin (10 µg/ml), collagen type I (10 µg/ml), fibronectin (10 µg/ml) or 1% BSA for 2 h at 37°C. Caki-1 cells were transfected with EGFP or EGFP-ANX AI (15S) for 24 h using Lipofectamine 2000 (Invitrogen, Karlsruhe, Germany) with a resulting transfection rate of approximately 50%. Then, cells were trypsinized and washed in the presence of soybean trypsin inhibitor. $1x10^5$ cells were placed on the top of the membrane and allowed to migrate towards vitronectin, collagen type I or fibronectin for 6 h at 37°C in migration buffer (RPMI 1640, 2 mM $CaCl_2$, 1 mM $MgCl_2$, 0.2 mM $MnCl_2$, 0.5% BSA). After fixation (4% formaldehyde in PBS) cells were counted using a fluorescence microscope (Inverted Microscope IX70, Olympus Optical, Melville, NY, USA). For a single determination, 3 wells per sample were used and 3 microscopic fields per well were counted (400-fold magnification). Random migration towards 1% BSA was substracted from the values. Transfection efficiency was counted in a fluorescence microscope and the number of the migrating cells was calibrated.

RNA isolation and RT-PCR

Tissue samples (approximately 100 mg) were homogenized in 1 ml TRIZOL®-Reagent (Invitrogen, Karlsruhe, Germany) using an Ultra-Turrax homogenizer. Isolation of RNA was performed according to the manufactures instructions. The resulting RNA pellet was air dried and dissolved in DEPC-H_2O. cDNA was generated by MMLV-reverse transcriptase (Promega) using 1 µg total-RNA. PCR was performed using specific ANX AI-primer (forward: 5'-AAC GCT TTG CTT TCT CTT G-3' and reversed 5'-CAC AAA GAG CCA CCA GGA TT-3'). PCR product size was 499 bp. PCR was running with 35 cycles. The PCR-products (20 µl) were separated using agarose-gel electrophoresis and ethidium bromide-stained bands were visualized by UV-illumination.

Statistical analysis

Statistical analysis used Kendall tau-c nonparametric coefficient of correlation to evaluate the relationship between (a) ANX AI score and tumour stage, (b) ANX AI score and Fuhrman grade and (c) ANX AI score and

amount of eosinophilic cells (Statistical program SPSS 14.0). The relation between ANX AI expression and clinical outcome was assessed with Kaplan-Maier analysis (Statistical Program SPSS 14.0). Follow-up data were available from 30 patients ranging from 4 months to 11 years. For cell migration assay, the mean value and standard error of the mean (SEM) of at least 3 independent experiments were calculated. Statistical analysis for cell migration assay was carried out using a paired t-test (confidence interval 95%; GraphPad Prism version 3.02 for Windows, GraphPad Software, San Diego, CA, USA, www.graphpad.com).

Results

Among 33 tumours investigated, 10 samples were pT1, 9 pT2, 12 pT3 and 2 pT4. 6 tumours were G1, 24 were G2 and 3 tumours were G3. The eosinophilic

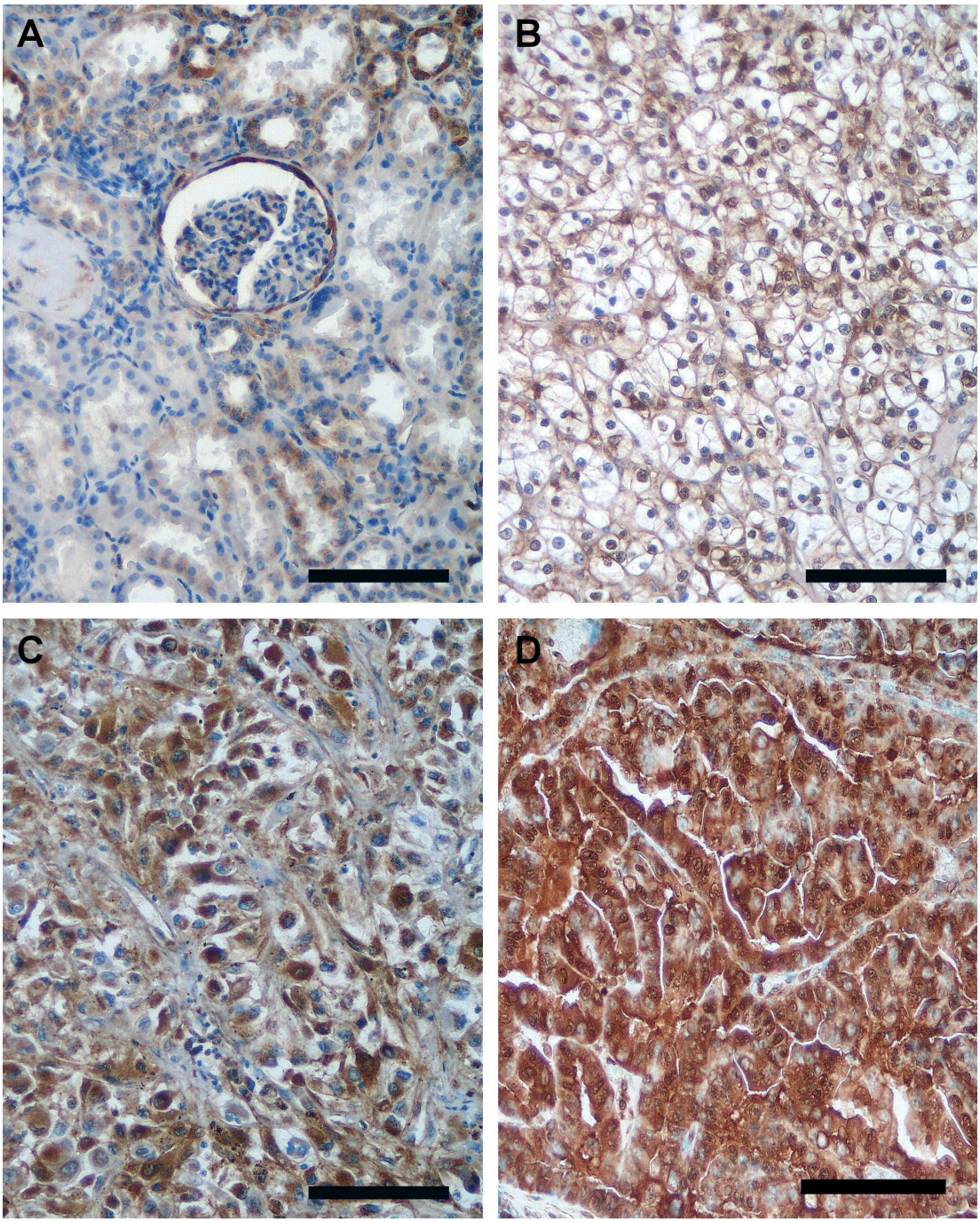

Fig. 1. Immunohistochemical detection of ANX AI. In non-neoplastic kidney immunoreactivity is seen at the distal tubules and Bowman's capsule (**A**), in CRCCs immunoreactivity is localized predominantly to the cell membranes (ANX score A1, **B**) or strongly at the cell membranes and in the cytoplasm (ANX score A2, **C**). The strong reaction in a lymph node metastasis is depicted in **D** (Bars represent 100 µm).

scores as assessed in H&E stained sections were E0 in 18, E1 in 8 and E2 in 7 samples.

Immunohistochemistry

In non-neoplastic tissue, ANX AI immunostaining was seen in Bowman's capsule, loop of Henle, collecting tubules and ducts. Immunostaining was stronger at the basolateral membranes compared to the cytoplasm. The proximal tubules were immunonegative (Fig. 1A). Within CRCC, immunoreactivity for ANX AI was heterogeneous and in most samples immunopositive cells were accumulated into foci. In 15 samples no immunoreaction of tumour cells was evident (score A0). 11 samples were judged A1 (Fig. 1B) and 7 samples were scored A2 (Fig. 1C). Among 10 patients with a tumour stage pT1, 3 samples were positive for ANX AI. Out of 9 pT2 tumours 5 showed an ANX I immunoreaction. Among 12 patients with a pT3 tumour stage 8 were ANX AI positive while both pT4 tumours were immunopositive also. There was a moderate correlation between tumour stage and ANX AI immunohistochemistry (Kendall tau-c = 0,3; p = 0,045; Tab. 1A). When comparing ANX AI immunohistochemistry and Fuhrman grade, 5 out of 6 G1 samples were judged A0 while one was A1. Among 24 G2 samples 10 were A0, 8 A1 and 6 A2 while 2 out of 3 G3 samples were A1 and 1 was A2, respectively. ANX AI score correlated to Fuhrman grade (Kendall tau-c = 0,3; p = 0.021; Tab. 1B). Comparison of ANX AI immunohistochemistry to the amount of eosinophilic cells revealed that out of 15 samples with A0, 12 samples scored E0, 2 E1 and 1 E2. Among 11 samples scored A1, 5 samples were E0, 5 E1 and 1 sample E2. In 5 out of 7 specimens judged A2 eosinophilic score was E2, 1 E1 and 1 specimen was E0. There was a significant relation between ANX AI score and eosinophilic score (Kendall-tau-c = 0.5; p < 0,001; Tab. 1C). Metastases were localized in lung (2), suprarenal gland (2), liver (2), bone (1), brain (1), lymphnode (1) and skin (1). In 8 samples ANX AI immunoreactivity was A1 and in 2 A2 (Fig. 1D). Although all metastases were strongly ANX AI positive, 4 corresponding primary tumours were ANX AI negative (A0). The comparison of ANX AI score and clinical outcome revealed that among 15 patients with ANX AI score A0, 8 had no evidence of disease (NED), 2 were alive with disease (AWD), 4 were dead of disease (DOD) and 1 lost to follow-up (LTF). From 11 patients scored A1, 3 were NED, 2 were AWD and 6 were DOD. Among seven patients with A2, 3 were DOD, 1 was NED, 1 AWD and 2 were LTF. The mean follow-up times were 38 months with a range from 4 to 132 months. There was a significant relation between the ANX AI score and clinical outcome (DOD) (Kaplan-Maier (log rank (Mantel Cox) p = 0.013). Data of statistical analysis are

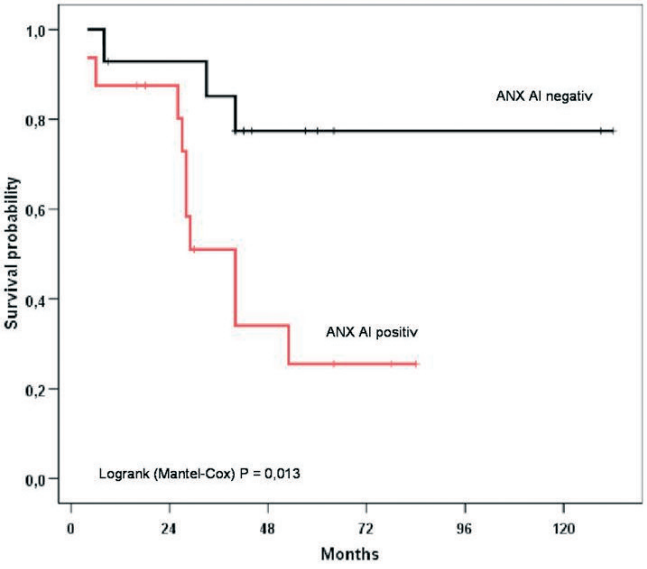

Fig. 2. Kaplan-Maier curves for ANX AI expression. ANX AI expression is significantly related to survival rate.

Table 1. Statistical calculation (Kendall tau-c) of comparison of ANX AI score with tumor Stage (A), Fuhrman grade (B) and eosinophilic cell score (C).

A

Kendall's tau c = 0,314 P = 0,045		ANX AI score			total
		0	1	2	
pT	1	7	2	1	10
	2	4	3	2	9
	3	4	5	3	12
	4	0	1	1	2
Total		15	11	7	33

B

Kendall's tau c = 0,298 P = 0,021		ANX AI score			total
		0	1	2	
Fuhrman grading	1	5	1	0	6
	2	10	8	6	24
	3	0	2	1	3
Total		15	11	7	33

C

Kendall's tau c = 0,496 P < 0,001		ANX AI score			total
		0	1	2	
Eosinophilic cell score	0	12	5	1	18
	1	2	5	1	8
	2	1	1	5	7
Total		15	11	7	33

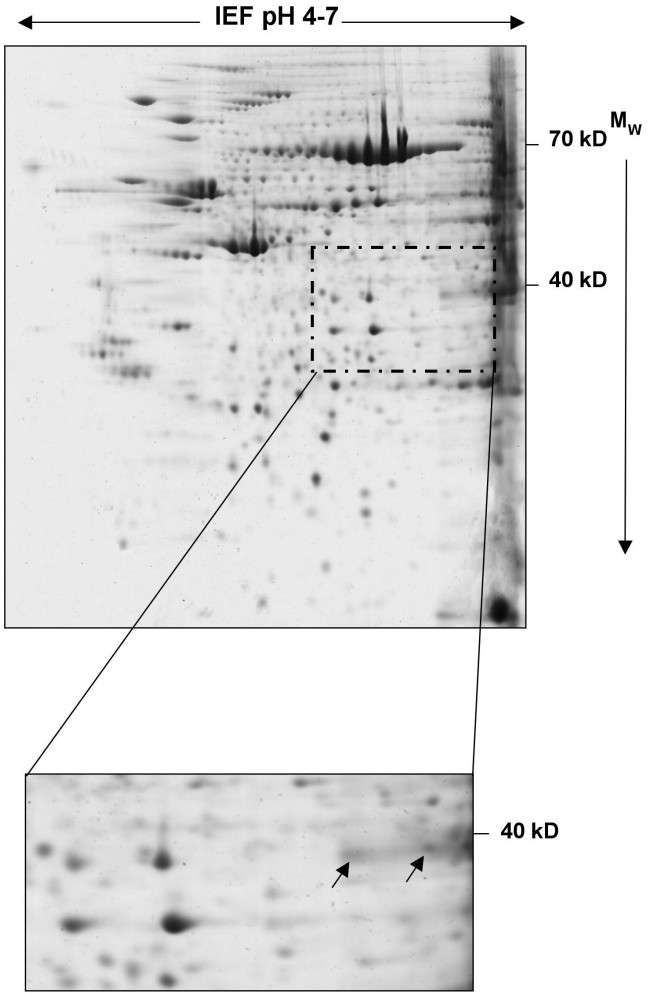

Fig. 3. Coomassie stained 2DE-gel (pH 4-7). Representative protein pattern of CRCC (**A**) with the enlarged region (**B**) of protein spots of ANX I AI (arrows).

given in table 1 A-C and Figure 2.

2-DE and mass spectrometry, RT-PCR, Cell migration assay

2-DE and mass spectrometry showed, on the basis of theoretical size and isoelectric point (pI), the presence of ANX AI in non-neoplastic and neoplastic samples. ANX AI was localised in the region of 6.5-7.0 with a molecular weight from about 39 kDa. The protein was identified with a score of 238 and sequence coverage of 59%. In neoplastic tissue, 2 spots revealed the presence of ANX AI (Fig 3). Additionally, we identified in neoplastic tissues, besides the spots of ANX AI, the glyceraldehyde-3-phosphate dehydrogenase, an enzyme of the glycolytic pathway. RT-PCR revealed the presence of ANX AI mRNA in non-neoplastic as well as in neoplastic tissue (Fig. 4). After overexpression of ANX AI, no influence on haptotactic cell migration towards the extracellular matrix protein (ECM) protein fibronectin could be detected (Fig. 5C). Cell migration towards vitronectin and collagen type I was slightly, but not significantly, increased (Fig. 5A, B). Thus, ANX AI is not involved in integrin ß1, ß3 or ß5-mediated cell migration in the renal carcinoma cell line Caki1.

Fig. 4. RT-PCR of representative non-neoplastic (lanes 1-4) and neoplastic samples (lanes 5-8) from 4 representative patients. Bands for ANX I AI are seen at 499 bp (M: molecular weight marker in bp).

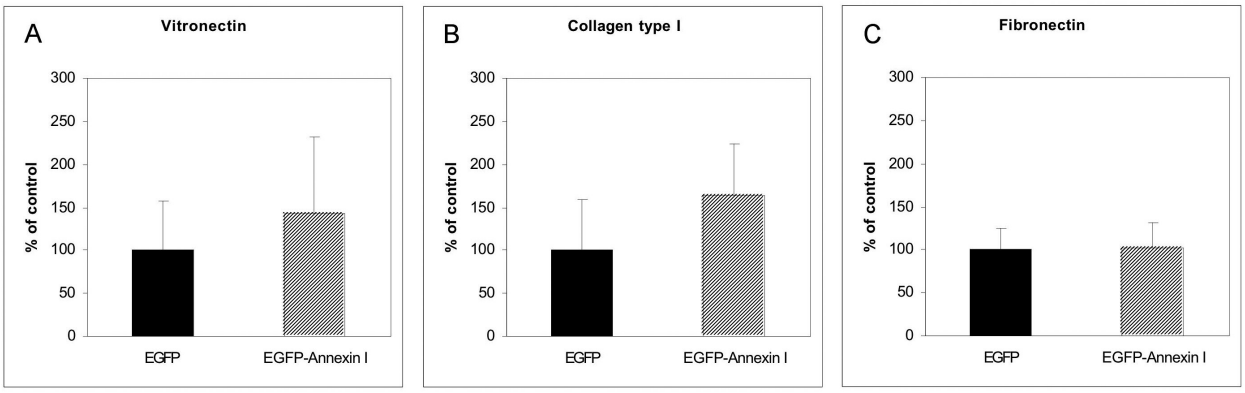

EGFP	100	58	EGFP	100	59,6	EGFP	100	25
EGFP-Annexin I	142,7	89,6	EGFP-Annexin I	163,2	61,1	EGFP-Annexin I	101,6	29,4

Fig. 5. Influence of overexpressed ANX AI on cell migration. Caki-1 cells were transiently transfected with pEGFP-Annexin I or pEGFP-N2 as a control and analysed by haptotactic cell migration towards vitronectin (**A**), collagen type I (**B**) or fibronectin (**C**). Data represent the results of at least three independent experiments and are given as mean values ± SEM.

Discussion

This study was done to evaluate the putative role of ANX AI in CRCCs. Immunohistochemistry revealed the expression of ANX AI in all metastases and predominantly in pT3 and pT4 tumours. The presence of ANX AI protein or mRNA was confirmed by 2DE with subsequent mass spectrometry and qualitative RT-PCR.

Previous studies on non-neoplastic tissue (Dreier et al., 1998) immunolocalized ANX AI in Bowman`s capsule, loop of Henle, collecting tubules and ducts, which is in complete accordance with our findings. CRCCs are often composed of clear or eosinophilic cells to varying extent, and the amount of eosinophilic cells is thought to indicate the degree of differentiation (Stoerkel et al., 1997; Reuter and Gaudin, 1999). In the present study we demonstrated a significant correlation between amount of eosinophilic cells, ANX AI score and Fuhrman grade. Therefore expression of ANX AI is most probably a feature of eosinophilic cells and thus characterizes the grade of tumour differentiation. This is underlined by the fact that, as speculated previously, the amount of eosinophilic cells was related to Fuhrman grade and thus to degree of differentiation as well as to unfavourable prognosis (Thoenes et al., 1986; Reuter and Gaudin, 1999). Furthermore, in accordance with these hypotheses, we were also able to show that ANX AI score correlates with tumour stage and clinical outcome. Consistently, ANX AI could serve as a useful prognostic marker for outcome of RCC. However, the biological function of ANX AI in renal cancer cells remains unclear. As we have hypothesized that ANX AI could affect cell migration, we studied the influence of ANX AI overexpression in Caki-1 cells. For this purpose, a bioactive ANX AI N-terminal fragment (15S) was used for migration experiments (Perretti et al., 2002). Interestingly, in contrast to our assumption, ANX AI overexpression did not significantly improve cell migration towards vitronectin, collagen type I and fibronectin. Therefore, we can suppose that ANX AI is involved most probably in other biological processes than migration. For instance, previous studies have demonstrated the upregulation of ANX AI during hepatocyte proliferation after partial hepatectomy. Moreover, the proliferation rate of non-neoplastic and neoplastic hepatocytes could be attenuated by antisense mRNA (De Coupade et al., 2000). Consistently, as all metastases were ANX AI positive in our study, we speculate that dedifferentiation and proliferation of tumour cells in CRRCs could be associated with increased ANX AI expression. Further investigations are needed to evaluate the hypothesis that expression of ANX AI is linked to cell proliferation rather than migratory potential.

As reported previously, ANX AI is located at cellular membranes or in the cytosol of different cell types (Traverso et al., 1998). In our study, immunoreactivity was more pronounced at the cell membranes of tumour cells when compared to non-neoplastic cells. This could possibly indicate a translocation of ANX AI. Interestingly, the cytokine interleukin 6 that is secreted either by renal tumour cells or tumour associated macrophages is involved in the translocation of ANX AI (Masamichi et al., 1998; Solito et al., 1998). A further hint for a translocation of ANX AI is given by the detection of two different ANX AI spots in 2DE. This could reflect a postranslational modification and 2 different localisation sites of the protein e.g. in the plamsa membranes and the cytosol of tumour cells.

Taken together, our study showed that (a) ANX AI is expressed in CRCCs and metastases, (b) the expression of ANX AI correlates with tumour stage, Fuhrman-grade, the amount of eosinophilic cells and clinical outcome (c) ANX AI overexpression did not affect cell migration in renal cell carcinoma cell line CAKI 1. In our opinion, the immunohistochemistry of ANX AI could provide a helpful marker for dedifferentiation of renal tumour cells. In further studies it should be elucidated if this protein can serve as an additional prognostic marker for the outcome of CRCCs.

References

Bradford M.M. (1976). A rapid and sensitive method for the quantification of microgram quantities of protein utilizing the principle of protein-dye binding. Anal. Biochem. 282, 248-254.

De Coupade C., Gillet R., Bennoun M., Briand P., Russo-Marie F. and Solito E. (2000). Annexin I expression and phosphorylation are upregulated during liver regeneration and transformation in antithrombin III SV40 large T antigen transgenic mice. Hepatology 31, 371-380.

Dreier R., Schmid K.W., Gerke V. and Riehemann K. (1998). Differential expression of annexins I, II and IV in human tissues: an immunohistochemical study. Histochem. Cell Biol. 110, 137–148.

Eymann C., Dreisbach A., Albrecht D., Bernhardt J., Becher D., Genter S., Tam le T., Buttner K., Buurman G., Scharf C., Venz S., Volker U. and Hecker M. (2004). A comprehensive proteome map of growing Bacillus subtilis cells. Proteomics 4, 2849-2876.

Fuhrman S.A., Lasky L.C. and Limas C. (1982). Prognostic significance of morphologic parameters in renal cell carcinoma. Am. J. Surg. Pathol. 6, 655–663.

Garcia Pedrero J.M., Fernandez M.P., Morgan R.O., Herrero Zapatero A., Gonzales M.V., Suarez Nieto C. and Rodrigo J.P. (2004). Annexin A1 down-regulation in head and neck cancer is associated with epithelial differention status. Am. J. Pathol. 164, 73-79.

Gerke V. and Moss S.E. (2002). Annexins: from structure to function. Physiol. Rev. 82, 331-371.

Gerke V., Creutz C.E. and Moss S.E. (2005). Annexins: Linking Ca2+ signalling to membrane Dynamics. Nat. Rev. Mol. Cell Biol. 6, 449-461.

Hayes M.J. and Moss S.E. (2004). Annexins and disease. Biochem. Biophys. Res. Commun. 322, 1166-1170.

Kang J.S., Calvo B.F., Maygarden S.J., Caskey J.L., Mohler J.L. and Ornstein D.K. (2002). Dysregulation of annexin I protein expression in high-grade prostatic intraepithelial neoplasia and cancer. Clin. Cancer Res. 8, 117-123.

Lehnigk U., Zimmermann U., Woenckhaus C. and Giebel J. (2005). Localisation of annexins I, II, IV and VII in whole prostate sections from radical prostatectomy patients. Histol. Histopathol. 20, 673-

680.

Masaki T., Tokuda M., Fujimura T., Ohnishi M., Tai Y., Miyamoto K., Itano T., Matsui H., Watanabe S. and Sogawa K. (1994). Involvement of annexin I and annexin II in hepatocyte proliferation: can annexins I and II be markers for proliferative hepatocytes. Hepatology 20, 425-435.

Masaki T., Tokuda M., Ohnishi M., Fujimura T., Miyamoto K., Itano T., Matsui H., Arima K., Shirai M., Maeba T., Sogawa K., Konishi R., Tanigushi K., Hatanaka Y., Hatase O. and Nishioka M. (1996). Enhanced expression of protein kinase substrate annexin in human hepatocellular carcinoma. Hepatology 24, 72-81.

Masamichi H., Fumio N., Akira T., Tomohiko A., Tadashi H. and Hiroshi N. (1998). Cytokine levels in cystic renal masses associated with renal cell carcinoma. J. Urol. 159, 1459-1464.

Perretti M., Ingegnoli F., Wheller S.K., Blades M.C., Solito E. and Pitzalis C. (2002). Annexin 1 modulates monocyte-endothelial cell interaction in vitro and cell migration in vivo in the human SCID mouse transplantation model. J. Immunol. 169, 2085-2092.

Rhee H.J., Kim G.Y., Huh J.W., Kim S.W. and Na D.S. (2000). Annexin I is a stress protein induced by heat, oxidative stress and sulhydryl-reactive agent. Eur. J. Biochem. 267, 3220-3225.

Reuter V.E. and Gaudin P.B. (1999). Adult renal tumors. In: Diagnostic surgical pathology. 3rd edn. Sternberg S. (ed). Lippincott Williams & Wilkins, Philadelphia. pp 1785-1824.

Sobin L.H. and Wittekind C. (2002). TNM classification of malignant tumours. 6th ed. Wiley-Liss, New York

Solito E., De Coupade C., Parente E., Flower R.J. and Russo-Marie F. (1998). IL-6 stimulates annexin 1 expression and translocation and suggest a new biological role as class II acute phase protein. Cytokine 10, 514-521.

Solito E., De Coupade C., Canaider S., Goulding N.J. and Perretti M. (2001). Transfection of annexin 1 in monocytic cells produces a high degree of spontaneous and stimulated apoptosis associated with caspase-3 activation. Br. J. Pharmacol. 133, 217-228.

Stoerkel S., Eble J.N., Adlakha K., Amin M., Blute M.L., Bostwick D.G., Darson M., Delahunt B. and Iczkowski K. (1997). Classification of renal cell carcinoma. Cancer 80, 987-989.

Thoenes W., Stoerkel S. and Rumpelt H.J. (1986). Histopathology and classification of renal cell tumours (adenomas, oncocytomas and carcinomas). The basic cytological and histomorphological elements and their use for diagnostics. Pathol. Res. Pract. 181, 125-143.

Traverso V., Morris J.F., Flower R.J. and Buckingham J. (1998). Lipocortin 1 (annexin 1) in patches associated with the membrane of lung adenocarcinoma cell line and in the cytoplasm. J. Cell Sci. 111, 1405-1418.

Unwin R.D., Harnden P., Pappin D., Rahman D., Whelan P., Craven R.A., Selby P.J. and Banks R.E. (2003a). Serological and proteomic evaluation of antibody responses in the identification of tumor antigens in renal cell carcinoma. Proteomics 3, 45-55.

Unwin R.D., Craven R.A., Harnden P., Hanrahan S., Totty N., Knowless M., Eardly I., Selby P.J. and Banks R.E. (2003b). Proteomic changes in renal cancer and co-ordinate demonstration of both the glycolytic and mitochondrial aspects of the Warburg effect. Proteomics 3, 1620-1632.

Vogelzang N.J. and Stadler M.M. (1998). Kidney cancer. Lancet 353, 1691-1696.

Wu C.M., Lee Y.S., Wang T.H., Lee Y.S., Kong W.H., Chen E.S., Wei L.S., Liang Y. and Hwang T.L. (2006). Identification of differential gene expression between intestinal and diffuse gastric cancer using cDNA microarray. Oncol. Rep. 15, 57-64.

Xia S.H., Hu L.P., Hu H., Ying W.T., Xu X., Cai Y., Han Y.L., Chen B.S., Wei F., Qian X.H., Cai Y.Y., Shen Y., Wu M. and Wang M.R. (2002). Three isoforms of annexin I are preferentially expressed in normal oesophageal epithelia but down-regulated in oesophageal squamous cell carcinoma. Oncogene 21, 6641-6648.

Zhang H., Li Z., Viklund E.K. and Stroemblad S. (2002). p21-activated kinase 4 interacts with integrin alpha v beta 5 and regulates alpha v beta 5-mediated cell migration. J. Cell Biol. 158, 1287–1297.

Zimmermann U., Woenckhaus C., Pietschmann S., Junker H., Maile S., Schultz K., Protzel C. and Giebel J. (2004). Expression of annexin II in conventional renal cell carcinoma is correlated with Fuhrman grade and clinical outcome. Virchows Arch. 445, 368-374.

Accepted November 29, 2006